Charge-transfer-induced suppression of galvanic replacement and synthesis of (Au@Ag)@Au double shell nanoparticles for highly uniform, robust and sensitive bioprobes

Dao Thi Ngoc Anh, Prerna Singh, Cheshta Shankar, Derrick Mott, and Shinya Maenosono[a)]
Japan Advanced Institute of Science and Technology, 1-1 Asahidai, Nomi, Ishikawa 923-1292, Japan

(Received 29 June 2011; accepted 25 July 2011; published online 16 August 2011)

The synthesis of double shell (Au@Ag)@Au nanoparticles is accomplished through suppression of the galvanic replacement reaction caused by an electron transfer phenomenon. The resulting nanoparticles are monodisperse with a thin and uniform second Au shell. These particles are ultimately expected to lead to sensitive probes for biomolecular sensing and diagnostics. © *2011 American Institute of Physics*. [doi:10.1063/1.3626031]

Gold (Au) and silver (Ag) nanoparticles (NPs) have intriguing optical properties that make them ideal candidates for use as probes in sensing and biodiagnostics applications.[1–3] These probes optical, stability, and biomolecular reactivity properties are expected to be optimized by coupling the two metals in a core@shell (Ag@Au) structure where the core Ag provides ideal optical properties and the Au shell imparts chemical stability and reactivity with sulfur containing biomolecules.[4,5] Despite the multitude of attempts to synthesize aqueous Ag@Au NPs, few attempts have succeeded in producing monodisperse NPs in terms of size, shape, and structure. The challenges associated with synthesizing Ag@Au particles primarily stem from the galvanic replacement reaction that occurs between aqueous Au and metallic Ag during the shell deposition procedure.[6,7] In fact, galvanic replacement has been extensively utilized to generate hollow nanostructures including hollow metal particles or gold nano-cages.[8,9] To synthesize monodispersed Ag@Au NPs, the galvanic replacement reaction should be suppressed or eliminated, which is a challenge.[10,11]

It has been reported that a charge compensation mechanism leads to a depletion of *d* electrons at the Au site accompanied by an increase in *d* electrons at the Ag site in the Au-Ag alloy.[12,13] Ag adatoms vapor-deposited onto a Pt(111) surface were found to increase *d* electron populations as indicated by the negative shift in the Ag $3d_{5/2}$ binding energy (BE).[14] Small Pt NPs dispersed on the surfaces of alkali metal titanate nanotubes ($M_2Ti_3O_7$, $M = Li^+$, Na^+, and K^+) exhibited a negative shift in the Pt 4f BE due to an electron donation from titanate nanotubes to Pt NPs yielding a negative Pt oxidation state.[15] Based on these results, we first synthesized monodispersed Au seeds, and then, deposited a Ag shell onto the Au seeds to form uniform Au@Ag core@shell NPs *via* seed-mediated growth. It is expected that the electronic and chemical properties of the Ag shell can be tuned by coupling the Ag shell to the Au core due to a charge transfer that increases electron density within the Ag shell yielding a negative Ag oxidation state which suppresses the galvanic replacement reaction at the Ag shell surface. Subsequently, we further deposited a Au second shell onto the Au@Ag NPs to form defect-free (Au@Ag)@Au double shell NPs, taking advantage of the suppressed galvanic replacement reactivity of the Ag intermediate shell.

Au NPs were synthesized by the citrate reduction method of Frens[16] and were used as seeds for the synthesis of Au@Ag core@shell NPs. The colloidal dispersion of Au seeds is a deep-red color with a localized surface plasmon resonance (LSPR) peak at 518 nm (Fig. S1) with a mean diameter, D, of 14.4 ± 0.7 nm (Fig. S2(a)). Next, a Ag shell was grown on the Au seeds *via* seed-mediated growth by adding silver precursor ($AgNO_3$) to the Au seed dispersion with additional sodium citrate at reflux, under an argon atmosphere. As a major advantage of the seed-mediated synthesis, the Ag shell thickness of the resulting Au@Ag core@shell NPs can be finely controlled by varying the amount of $AgNO_3$ added to the reaction solution. The thickness of the Ag shell for these Au@Ag NPs increased by varying the volume of $AgNO_3$ (20 mM) added from 0.3, 0.7, 1.8 to 3.2 mL. In total, four different Ag shell thicknesses were obtained, including 0.4 ± 0.3, 1.0 ± 0.6, 2.2 ± 0.4, and 3.6 ± 0.4 nm (Fig. S2 and Table S1), which corresponds very closely to the theoretical shell thickness (0.45, 1.09, 2.29, and 3.48 nm, respectively) calculated from the metallic feeding ratio. The shell thicknesses were estimated by subtracting the mean diameter of core NPs from those of core@-shell NPs. The Ag shell thickness is expressed in the subscript hereafter, e.g., Au@Ag_x; x denotes the Ag shell thickness. The resultant Au@Ag NPs are highly monodisperse in terms of size and shape in comparison to Ag NPs synthesized by comparable reduction methods.

The UV-visible (UV-Vis) spectra of Ag ($D = 17.1 \pm 2.2$ nm) and Au@$Ag_{3.6}$ ($D = 21.6 \pm 0.9$ nm) NPs are shown in Fig. S1. The UV-Vis spectra of all Au@Ag core@shell NPs are shown in Fig. S3. The transmission electron microscopy (TEM) image of Au@$Ag_{3.6}$ is shown in Fig. S2(e). When x was increased, the LSPR band gradually became blue-shifted, with the LSPR peak of Ag eventually becoming dominant. Finally, the Au@$Ag_{3.6}$ NPs show a single LSPR peak at 390 nm, which stems from the plasmon resonance of the Ag shells, as shown in Fig. S1. The appearance of a monomodal LSPR band corresponding to Ag indicates that the Au cores are uniformly covered by the Ag shell and the optical contribution from the Au cores is completely screened. However, Ag NPs of a similar size typically show

[a)]Electronic mail: shinya@jaist.ac.jp.

a LSPR peak at 415 nm as seen in Fig. S1.[2,10] The significant blue-shift of the LSPR peak appearing in the Ag shell of the Au@Ag core@shell NPs suggests a higher electron density in the Ag shells than that of pure Ag NPs due to an electron transfer from the Au core to the Ag shell.[17]

Finally, the Au second shell was deposited onto the Au@$Ag_{3.6}$ core@shell NPs by adding $HAuCl_4$ with additional sodium citrate, at reflux, to form (Au@$Ag_{3.6}$)@Au double shell NPs. After being coated by the second Au shell (theoretical thickness 0.15 nm), the LSPR peak is slightly red-shifted by about 10 nm indicating the formation of a thin Au shell onto the Ag surface (Fig. S1). In Fig. 1(b), a TEM image of (Au@$Ag_{3.6}$)@Au double shell NPs is shown. The (Au@$Ag_{3.6}$)@Au double shell NPs are more uniform in size and shape (Figs. 1(a) and 1(b)) when compared to typical Ag@Au NPs.[18] Moreover, they have no observable gaps or defects in the particle structure. To further confirm the formation of the Au second shell, scanning TEM-high angle annular dark field (STEM-HAADF) imaging and energy dispersive x-ray spectroscopy (EDS) elemental mapping were carried out for the (Au@$Ag_{3.6}$)@Au double shell NPs using a JEOL JEM-ARM200F instrument operated at 200 kV with a spherical aberration corrector (nominal resolution 0.8 Å). Figure 1(c) shows the STEM-HAADF image (high Z contrast) of the (Au@$Ag_{3.6}$)@Au double shell NPs. Since the heavier Au atoms (atomic number, $Z = 79$) give rise to a brighter image than the lighter Ag atoms ($Z = 47$) in the dark field image, the Au core appears brighter than the Ag first shell.

One can see a very bright eggshell-thin layer on the Ag first shell (Fig. 1(c)). The thickness of the layer is 0.11 nm, which agrees well with the theoretical value (0.15 nm) calculated based on the amount of Au precursor added. This indicates that a thin Au second shell was formed on the Au@$Ag_{3.6}$ NPs. The EDS mapping result (Figs. 1(d)–1(f)) also clearly indicates that the resulting NPs have a (Au@$Ag_{3.6}$)@Au double shell structure. While the outermost Au shell is only 1-2 Au atomic layers thick, the interdiffusion of Au and Ag atoms could occur resulting in a Au-Ag alloy. For this reason, we deposited a thicker Au second shell with 1.2 nm theoretical thickness to further probe the characteristics of the second shell. Figure S4 shows the STEM-HAADF and the EDS mapping images of the double shell NPs. The mean diameter of the resulting NPs is 23.0 ± 1.9 nm, which agrees well with the theoretical value (23.2 nm) calculated based on the amount of Au precursor added. This means that the Ag first shell was not etched away during the deposition of the Au second shell. As can be clearly seen in Fig. S4, the resulting NPs display a double shell structure with defect-free Au second shells.

In order to confirm the occurrence of the charge transfer effect, we carried out x-ray photoelectron spectroscopy (XPS) measurements for Au@Ag_x and (Au@$Ag_{3.6}$)@Au NPs in comparison with pure Ag and Au NPs. Figures 2(a) and 2(b) show high resolution XPS core-level spectra of Ag, Au@Ag_x, and (Au@$Ag_{3.6}$)@Au double shell NPs. The Ag 3d core levels are split into $3d_{3/2}$ and $3d_{5/2}$ spin-orbit pairs (Fig. 2(a)). Taking a closer look at the asymmetrically broadened $3d_{5/2}$ component, the overlapping peaks were deconvoluted by using two Gaussian functions corresponding to Ag^0 and Ag-Au alloy (or Ag oxide) components. In the case of pure Ag NPs, the $3d_{5/2}$ component could be deconvoluted into Ag^0 (peak at 368.26 eV) and Ag oxide (peak at 367.80 eV) as shown in Fig. 2(b). On the other hand, in the cases of Au@Ag_x NPs, the $3d_{5/2}$ component could be divided into Ag^0 (peak at 368.18 ± 0.03 eV) and Ag-Au alloy (peak at 368.50 ± 0.03 eV) (Fig. 2(b)). Importantly, no Ag oxide peak exists in the Au@Ag_x NPs even though the Ag first shell is exposed to the outside. The Ag-Au alloy could be formed at the interface between the Au core and the Ag shell. Note that, a similar trend is also observed for the Ag $3d_{3/2}$ component. The Ag^0 $3d_{5/2}$ peak energy is plotted as a function of x as shown in Fig. 2(c). All Au@Ag_x NPs exhibit a negative shift in the Ag^0 $3d_{5/2}$ BE compared to that of pure Ag NPs (368.26 eV). Moreover, the Ag^0 $3d_{5/2}$ BE increases toward the value of pure Ag NPs with increasing x when $x \geq 1.0$ suggesting that the charge transfer takes place only in the vicinity of the interface between the Au core and the Ag shell. Interestingly, the deposition of the second Au shell onto the Ag surface again causes the reduction of Ag^0 $3d_{5/2}$ BE indicating an electron transfer between the Au second shell and the Ag first shell. It is worth noting that all Au@Ag_x NPs exhibit a

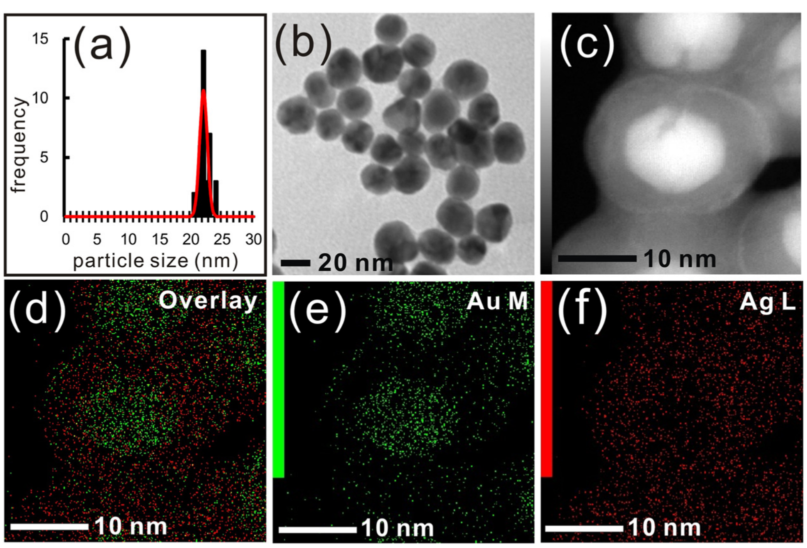

FIG. 1. (Color online) Size distribution (a) and TEM images (b) of (Au@$Ag_{3.6}$)@Au double shell NPs. (c) STEM-HAADF image of (Au@$Ag_{3.6}$)@Au NPs. (d)-(f) EDS elemental mapping images of (Au@$Ag_{3.6}$)@Au NPs: Overlay (d) of Au M edge (e) and Ag L edge (f).

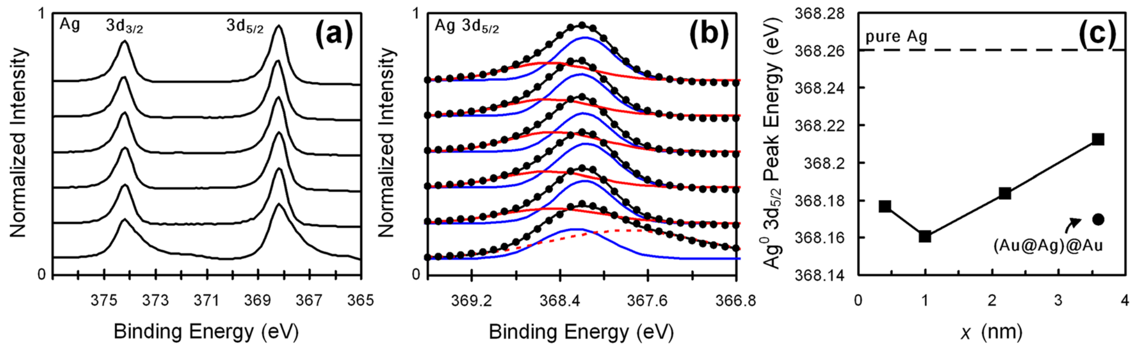

FIG. 2. (Color online) (a) XPS spectra of Ag, Au@Ag_x ($x = 0.4$, 1.0, 2.2, and 3.6), and (Au@$Ag_{3.6}$)@Au double shell NPs, respectively from the bottom to top. (b) Magnified XPS spectra focusing on the Ag $3d_{5/2}$ peak (circles). The peaks were deconvoluted by using two Gaussian functions corresponding to Ag^0 (blue curves) and Ag-Au alloy (red curves) [or Ag oxide (red dashed curve)] components. Solid black curves represent the sum of two Gaussian curves. (c) The Ag^0 $3d_{5/2}$ peak energy plotted as a function of the Ag shell thickness, x.

positive shift in the Au 4f BE (ca. 0.1 eV) compared to that of pure Au NPs as shown in Fig. S5. An expanded explanation of the relationship between charge transfer and suppression of the galvanic replacement reaction is included in the supplementary information.[19]

If the Ag first shell has a negative oxidation state and the oxidation resistivity is enhanced, the chemical stability of Au@Ag_x NPs to electrolytes is expected to also be improved. Therefore, the chemical stability of Au@$Ag_{3.6}$ NPs is compared to that of pure Ag NPs in the presence of NaCl (8.2 mM). As a result, it was found that the Au@$Ag_{3.6}$ NPs preserved their morphology 3 h after the addition of NaCl into the aqueous NP dispersion even while some local defects occurred (Figs. S6(b) and S7(a)), while the Ag NPs were totally destroyed under identical conditions (Fig. S6(a)). However, the mean size of Au@$Ag_{3.6}$ NPs decreased down to 16.4 ± 1.6 nm. This means that nearly 80% of the Ag shell was etched away. In the case of (Au@$Ag_{3.6}$)@Au double shell NPs, their morphology was completely preserved (Figs. S6(c) and S7(b)), likely because the (Au@$Ag_{3.6}$)@Au NPs have a more negative Ag oxidation state than Au@Ag_x NPs and/or the Au second shell effectively protects the Ag first shell from contact with Cl^- ions suggesting that the chemical stability of the (Au@$Ag_{3.6}$)@Au NPs is extremely high even under severe conditions. The mean size of (Au@$Ag_{3.6}$)@Au NPs did not change before and after NaCl addition (Table S2).

Finally, the surface enhanced Raman scattering (SERS) activity of core@shell NPs was investigated using 3-amino-1,2,4-triazole-5-thiol (ATT) as a dual linker and reporter molecule using the same protocol reported previously.[20] The SERS activity was found to dramatically increase with increasing x in the case of the Au@Ag_x NPs as shown in Fig. S8 taking advantage of high extinction coefficients and extremely high field enhancements of Ag. Moreover, the (Au@$Ag_{3.6}$)@Au NPs exhibited a SERS activity as high as Au@$Ag_{3.6}$ NPs. This result is consistent with previous results; namely, the SERS activities of Ag and Ag@Au NPs are almost equivalent when ATT molecules are used for assembling NPs to form hot spots.[20]

In summary, we have found that an electron transfer from the Au core to the Ag shell takes place in Au@Ag core@shell NPs resulting in an enhancement of the oxidation resistivity of the Ag shell. The enhanced oxidation resistivity of the Ag shell effectively suppresses the galvanic replacement reaction during the Au second shell deposition process, and thus, the resultant (Au@Ag)@Au double shell NPs have a uniform size, shape, and structure without defects which cannot be avoided in the case of Ag@Au NP syntheses. Using the charge-transfer-induced electronic modification technique, one can synthesize well-defined core@shell NPs which have not been achieved until now. The (Au@Ag)@Au double shell NPs are highly stable in presence of salt with high Raman activity. These particles are ultimately expected to lead to a future class of highly active and stable nanoprobes for biomolecular sensing and diagnostics. The ongoing work includes further study on the origin and factors that govern the charge transfer phenomenon.

[1] K. J. Lee, P. D. Nallathamby, L. M. Browning, C. J. Osgood, and X. H. N. Xu, ACS Nano **1**, 133 (2007).
[2] S. E. Skrabalak, J. Chen, L. Au, X. Lu, X. Li, and Y. Xia, Adv. Mater. **19**, 3177 (2007).
[3] Z. Zhang, J. Jia, Y. Lai, J. Weng, and L. Sun, Bioorg. Med. Chem. **18**, 5528 (2010).
[4] I. S. Šloufová, B. Vlčková, Z. Bastl, and T. L. Hasslett, Langmuir **20**, 3407 (2004).
[5] Y. Yang, J. Shi, G. Kawamura, and M. Nogami, Scripta Mater. **58**, 862 (2008).
[6] Y. Bi, H. Hu, and G. Lu, Chem. Commun. **46**, 598 (2010).
[7] A. Pearson, A. P. O'Mullane, V. Bansal, and S. K. Bhargava, Chem. Commun. **46**, 731 (2010).
[8] Y. Sun and Y. Xia, Science **298**, 2176 (2002).
[9] S. E. Skrabalak, J. Chen, Y. Sun, X. Lu, L. Au, C. M. Cobley, and Y. Xia, Acc. Chem. Res. **41**, 1587 (2008).
[10] D. Mott, T. B. T. Nguyen, Y. Aoki, and S. Maenosono, Philos. Trans. R. Soc. A **368**, 4275 (2010).
[11] D. Mott, J. D. Lee, T. B. T. Nguyen, Y. Aoki, P. Singh, and S. Maenosono, Jpn. J. Appl. Phys. **109**, 094301 (2011).
[12] C. C. Tyson, A. Bzowski, P. Kristof, M. Kuhn, R. Sammynaiken, and T. K. Sham, Phys. Rev. B **45**, 8924 (1992).
[13] R. K. Roy, S. K. Mandal, and A. K. Pal, Eur. Phys. J. B **33**, 109 (2003).
[14] J. A. Rodriguez and M. Kuhn, J. Phys. Chem. **98**, 11251 (1994).
[15] C.-Y. Hsu, T.-C. Chiu, M.-H. Shih, W.-J. Tsai, W.-Y. Chen, and C.-H. Lin, J. Phys. Chem. C **114**, 4502 (2010).
[16] G. Frens, Nature **241**, 20 (1973).
[17] P. Mulvaney, T. Linnert, and A. Henglein, J. Phys. Chem. **95**, 7843 (1991).
[18] L. Quian and X. Yang, Colloids Surf. A **260**, 79 (2005).
[19] See supplementary material at http://dx.doi.org/10.1063/1.3626031 for experimental details, UV-Vis spectra, HR-TEM images, STEM images, EDS mapping images, Au 4f core-level XPS spectra, TEM images of NPs 3 h after adding NaCl, and Raman spectra.
[20] P. Singh, N. T. B. Thuy, Y. Aoki, D. Mott, and S. Maenosono, J. Appl. Phys. **109**, 094301 (2011).